

Geophysical Research Letters[®]

RESEARCH LETTER

10.1029/2021GL097178

Key Points:

- Chemical reactions between water and a model basalt were investigated in laser-heated diamond anvil cells under lower mantle conditions
- A new Al-rich niccolite-type silica containing ~24.4 to 32.4 wt% Al₂O₃ was identified, coexisting with Al-depleted bridgmanite, δ-phase, and iron-rich phase
- Infrared spectroscopy showed that Al-rich niccolite-type silica contains structural water

Supporting Information:

Supporting Information may be found in the online version of this article.

Correspondence to:

L. Liu and H. Yuan,
lu.liu@hpstar.ac.cn;
hongsheng.yuan@hpstar.ac.cn

Citation:







Liu, L., Yuan, H., Yao, Y., Yang, Z., Gorelli, F. A., Giordano, N., et al. (2022). Formation of an Al-rich niccolite-type silica in subducted oceanic crust: Implications for water transport to the deep lower mantle. *Geophysical Research Letters*, 49, e2021GL097178. <https://doi.org/10.1029/2021GL097178>

Received 23 NOV 2021

Accepted 26 JUL 2022

Formation of an Al-Rich Niccolite-Type Silica in Subducted Oceanic Crust: Implications for Water Transport to the Deep Lower Mantle

HPSTAR
1510-2022

Lu Liu^{1,2} , Hongsheng Yuan¹ , Yao Yao^{1,3}, Ziqiang Yang¹, Federico Aiace Gorelli^{1,4} , Nico Giordano⁵ , Lixin He², Eiji Ohtani⁶ , and Li Zhang¹ 

¹Center for High Pressure Science and Technology Advanced Research (HPSTAR), Shanghai, China, ²School of Physical Sciences, University of Science and Technology of China, Hefei, China, ³School of Earth and Space Sciences, Peking University, Beijing, China, ⁴National Institute of Optics (INO-CNR), European Laboratory for Non-Linear Spectroscopy (LENS), Sesto Fiorentino, Italy, ⁵Deutsches Elektronen-Synchrotron DESY, Hamburg, Germany, ⁶Department of Earth Science, Graduate School of Science, Tohoku University, Sendai, Japan

Abstract Subducted oceanic crust is enriched in free silica. Although being one of the silica polymorphs at lower-mantle pressures, niccolite-type phase (Nt-phase) has not been documented in multicomponent metabasaltic or metasediment compositions relevant to subducting oceanic crust. Here, we report the formation of an Al-rich Nt-phase (~24.4 to 32.4 wt% Al₂O₃), coexisting with Al-depleted bridgmanite (~6.4 to 7.6 wt% Al₂O₃), δ-phase, and iron-rich phase in model hydrated basalts over the pressure-temperature range of 84–113 GPa and 1,800–2,200 K. Infrared spectroscopy of a pure synthetic Al-rich Nt-phase shows OH bending and stretching vibrations at high pressures, indicative of its hydrous nature. This study suggests that Al-rich Nt-phase can serve as a potential water carrier in subducted oceanic crust to the deep lower mantle.

Plain Language Summary Water is transported into Earth's interior via subduction of hydrated lithospheric plates. The water distribution in peridotitic and basaltic portion of subducted hydrated slabs is heterogeneous, which is dependent on the stability of water-bearing minerals under the imposed pressure-temperature and local mineralogical conditions. The aim of this study is to provide an understanding regarding the host for water transport within the subducted oceanic crust in the deep lower mantle. To this end, we performed high pressure-temperature experiments on model hydrated basaltic rocks in a laser-heated diamond anvil cell. Compared with the formation of CaCl₂-type silica in dry oceanic basalts from previous studies, a new water-bearing Al-rich niccolite-type silica has been discovered in the present study. Our results imply that Al-rich niccolite-type silica can potentially carry water to the deep lower mantle in subducted oceanic crust.

1. Introduction

High-resolution seismic tomography images show that subducting slabs can penetrate into the lower mantle and in some cases reach to the core-mantle boundary (Grand, 2002; Zhao, 2012). Billions of years of plate tectonics may allow a certain amount of water to be delivered into Earth's interior primarily by subduction of hydrated lithospheric plates (Ohtani, 2020; Ohtani et al., 2018; Walter, 2021). The recent discoveries of phase Egg (AlSiO₄H) (Wirth et al., 2007), ice VII (Tschauner et al., 2018), and hydrous ringwoodite containing ~1 wt% water (Pearson et al., 2014) as inclusions in sub-lithospheric diamonds prove the existence of at least several locally wet regions in the transition zone and shallow lower mantle. Accordingly, it is of great importance to constrain the host for deep water transport in realistic subducting slab compositions for better understanding of the global water circulation and storage.

Subducted lithospheric plates consist of ocean sediments, basaltic oceanic crust and peridotitic mantle. The peridotitic component in cool subduction zones may inject water into the deep Earth's interior via dense hydrous aluminosilicate phases (Iwamori, 2004; Ohtani, 2021). In particular, phase D (nominally MgSi₂O₆H₂) will break down into phase H (nominally MgSiO₄H₂) + stishovite at pressures above 48 GPa in the coldest interiors of the lithosphere. At high pressures, δ-AlO₂H, ε-FeO₂H, and phase H adopt the identical CaCl₂-type structure (space group: *Pnmm*) with the potential to generate extensive hydroxide solid solution (hereafter, δ-phase) (Kawazoe et al., 2017; Nishi et al., 2019; Ohira et al., 2014). Indeed, high-pressure experiments in model hydrated mafic

rocks reveal that δ -phase $(\text{Al,Fe})\text{O}_2\text{H-MgSiO}_4\text{H}_2\text{-SiO}_2$ hydroxides can coexist with the major mantle mineral, bridgmanite (Bdg), or post-perovskite, throughout the mantle depth range (Nishi et al., 2019; Ohira et al., 2014; Yuan et al., 2019).

Basaltic oceanic crust is estimated to contain up to ~20 wt% free silica in the lower mantle (Hirose et al., 2005; Perrillat et al., 2006; Ricolleau et al., 2010). With an addition of Al_2O_3 (e.g., 4.4 wt%) in stishovite, water solubility of Al-bearing stishovite can be effectively promoted (e.g., ~0.3 wt% water at 20 GPa and 1675 K, Litasov et al., 2007). By *ex situ* analysis of silica samples synthesized by multi-anvil apparatus, studies have shown that Al-free stishovite can contain 3–72 ppm wt% water at 10–24 GPa and 1475–2025 K (Bolfan-Casanova et al., 2000; Bromiley et al., 2006; Litasov et al., 2007; Pawley et al., 1993), while its water storage capability is significantly elevated up to ~1.3 wt% water at 10 GPa and 625–825 K (Spektor et al., 2011). Recent *in situ* high pressure-temperature (*P-T*) X-ray diffraction (XRD) studies in a laser-heated diamond anvil cell (DAC) by Lin et al. (2020) and Nisir et al. (2020) suggested that weight percent levels of H_2O could be incorporated in stishovite even at temperatures along a mantle geotherm in the shallow and middle lower mantle. Such an ultrahydrous stishovite was supported by observations of anomalous unit-cell volume expansion compared to dry stishovite at high pressure. Based on decompression data, Lin et al. (2020) further suggested that water in ultrahydrous stishovite may not be fully quenchable. As such, characterization under different *in situ* and *ex situ* pressure conditions may explain the discrepancy in water solubility in stishovite. In addition, Nisir et al. (2020) reported that a hydrous Al-free NiAs-type silica (Nt-phase) can be formed in a water-rich environment under modest *P-T* conditions corresponding to the middle or deep lower mantle. However, such a Nt-phase has not been observed in multicomponent systems relevant to realistic mantle and subducting slab compositions.

With potential changes in mineralogy in subducted crust, the fate and role of hydrated silica minerals throughout the lower mantle *P-T* range is still unknown. To provide an understanding of the host for water transport in the subducted oceanic crust downwards to the deep lower mantle, we conducted high *P-T* experiments on model hydrated basalt in a laser-heated DAC. Phase assemblages were determined by the combined high-*P* XRD and chemical analysis with transmission electron microscopy (TEM) on recovered samples.

2. Methods

The starting materials were gel samples with the bulk composition of 24.9 mol% MgO-12.8 mol% Al_2O_3 -7.5 mol% Fe_2O_3 -54.8 mol% SiO_2 containing two different water contents of ~4 wt% (MAFSH-a) and ~1 wt% (MAFSH-b), respectively. The pre-compressed sample disk (~10 μm in thickness) was positioned on a small step in the gasket to maintain space between the sample and both diamond culets (~10 μm on each side), as described in the study of Yuan et al. (2019). Neon served as the pressure medium, thermal insulator and pressure calibrant and was loaded using a gas-loading system. Samples were compressed to target pressure and then heated to target temperature for 10–12 min by double-sided laser heating with 1,064-nm Ytterbium fiber lasers. The heating temperature was determined by fitting the visible portion of the gray-body radiation from both sides of the heated sample to the Planck radiation function. The precision in measured temperature is less than 5 K based on the goodness of the curve fits. Temperature gradients were minimized by heating the homogenous Fe-bearing sample directly between the Ne insulator layers without an additional laser absorber. The diameter of the heating spot was ~20 to 30 μm . Mean temperatures were recorded across a ~10 μm strip (at 2 μm intervals) at the heating center, and *T* differences were ~50 to 100 K. We adjusted the respective laser powers on either side of the DAC during the course of the experiment to maintain temperature variations within 200 K (± 100 K).

Synchrotron XRD experiments were conducted on the samples after laser heating treatment at the P02.2 beamline of Petra III, Deutsches Elektronen Synchrotron (Konôpková et al., 2021) and the 15U1 beamline of Shanghai Synchrotron Radiation Facility (SSRF) (L. L. Zhang et al., 2015). Multigrain XRD was used to identify the phases and determine the unit-cell parameters (L. Zhang et al., 2019). Chemical analysis was performed on the recovered samples. The heating center was determined by two-dimensional XRD scans as well as their textures by electron microscopy. A cross section was lifted from the heating center and thinned to about 100 nm in thickness using an FEI Versa-3D SEM coupled with a focused ion beam. Elemental mapping images were then obtained using an FEI Talos F200X field emission TEM operating at 200 kV equipped with a SuperX coupled with energy dispersive X-ray spectroscopy (EDS).

Table 1
Experiments Conditions and Results

| Run# | $P_{300\text{K}}$ (GPa) ^a | P_T (GPa) ^b | T (K) | Phase assemblage (XRD) ^c |
|------------------------------------|--------------------------------------|--|------------|---|
| MAFSH-a (~4 wt% H ₂ O) | | | | |
| Sb397 ^d | 73.3(3) | 84(1) | 2,000(100) | δ, Bdg, Nt, HH1 |
| | Ambient | | | δ, Bdg |
| Sb430 | 77.3(2) | 87(1) | 1,800(100) | δ, Bdg, Nt, HH1 |
| Sb335 | 84.9(3) | 97(1) | 2,200(100) | δ, Bdg, Nt, Ct, pPv-Fe ₂ O ₃ |
| Sb307 | 101.7(3) | 113(1) | 2,200(100) | δ, Bdg, Nt, HH1, pPv-Fe ₂ O ₃ |
| MAFSH-b (~1 wt% H ₂ O) | | | | |
| Sa1011 | 73.6(2) | 84(1) | 2,000(100) | δ, Bdg, Nt, Ct |
| ASH (~4 wt% H ₂ O) ± Au | | | | |
| Sb393 | 80.0(2) | 91(1) | 1,800(100) | Nt |
| | 3.2(1) | Cold decompression | | Nt |
| Sb185 ^e | 1 MPa to 78(2) ^f | Cold compression (IR) | | Hydrous amorphous ASH |
| | 82.8(2) | CO ₂ laser heating (IR + XRD) | | Nt |
| | 82.8(2) to 3.0(2) ^f | Cold decompression (IR) | | Nt |

^a $P_{300\text{K}}$ was post-heating pressure and determined by the equation of state of Ne (Fei et al., 2007) or Ar (Finger et al., 1981) or Au (Fei et al., 2007). ^bPressure at high temperature (P_T) in this study was estimated as $P_T = P_{300\text{K}} + (T - 300) \times 0.0062$ (GPa) from a previous study under similar P - T conditions (Yuan et al., 2019), and P uncertainty was derived from temperature uncertainty. ^cBdg = bridgmanite; Ct = CaCl₂-type silica; δ = CaCl₂-type Al-rich hydroxide; Nt = niccolite-type silica; HH1 = HH1-phase; pPv-Fe₂O₃ = post-perovskite-type Fe₂O₃. ^dThis experimental run was used in our recent paper (L. Liu et al., 2022) to show the existence of HH1-phase using different starting materials. ^eType IIa diamonds were used in Run Sb185 for infrared (IR) measurements. X-ray diffraction (XRD) experiments were conducted in all the other runs. ^fPressures were determined based on the Raman shift of diamond edge with the uncertainty of 0.2–2 GPa (Akahama & Kawamura, 2004).

Subsequent infrared (IR) spectroscopy experiments were performed on a third gel sample with the bulk composition of 17.8 mol% Al₂O₃-82.2 mol% SiO₂ containing ~4 wt% water (ASH). The pre-compressed sample disk (~10 μm in thickness) was positioned on the ruby ball spacers on the diamond anvil. Argon was loaded as the thermal insulator and pressure calibrant. IR measurements were conducted at HPSTAR using a commercial IR setup with a Bruker VERTEX-70v spectrometer and HYPERION 2000 microscope and at 06B beamline of SSRF using a custom IR/Raman setup developed by HPSTAR with a Bruker VERTEX-80v spectrometer. The spectra were collected in transmission mode in the range of 600–12,000 cm⁻¹ with a resolution of 2 cm⁻¹. The slits were set to 40 × 40 μm² in order to measure the absorption of the sample only. The absorption of the empty DAC at ambient conditions was used as the reference spectrum. Note that this correction leads to the observation of some artifacts and background at high pressure (see the main text). For comparison, high-pressure IR measurements were performed on the starting ASH gel sample up to 78 GPa at room temperature. The high-pressure sample was then directly heated by a one-sided CO₂ laser system at HPSTAR (Text S1 in Supporting Information S1). As temperature could not be estimated in real time, the heating conditions were explored by adjusting the laser power each time until the pure Al-rich Nt-phase was successfully synthesized as confirmed by the post-heating XRD results measured at SSRF (Figure S4 in Supporting Information S1). Typical IR spectra of the pure Al-rich Nt-phase were then recorded during cold decompression to 3 GPa. Furthermore, the ASH + Au mixture (Run# Sb393) was used to synthesize the pure Al-rich Nt-phase in the near IR laser heating system. The XRD pattern collected at ~3 GPa after the room temperature decompression shows that the structure of the Al-rich Nt-phase is preserved (Figure S5 in Supporting Information S1).

3. Results and Discussion

High P - T experiments were carried out on the model hydrated basalt sample (MAFSH-a, containing ~4 wt% H₂O), and XRD measurement were performed at high pressure and room temperature to identify the phase relations (Table 1). In dry basaltic compositions (Hirose et al., 2005; Perrillat et al., 2006; Ricolleau et al., 2010), a free silica phase (~20 wt% in proportion) is expected to be present with the characteristic diffraction(s) in pronounced

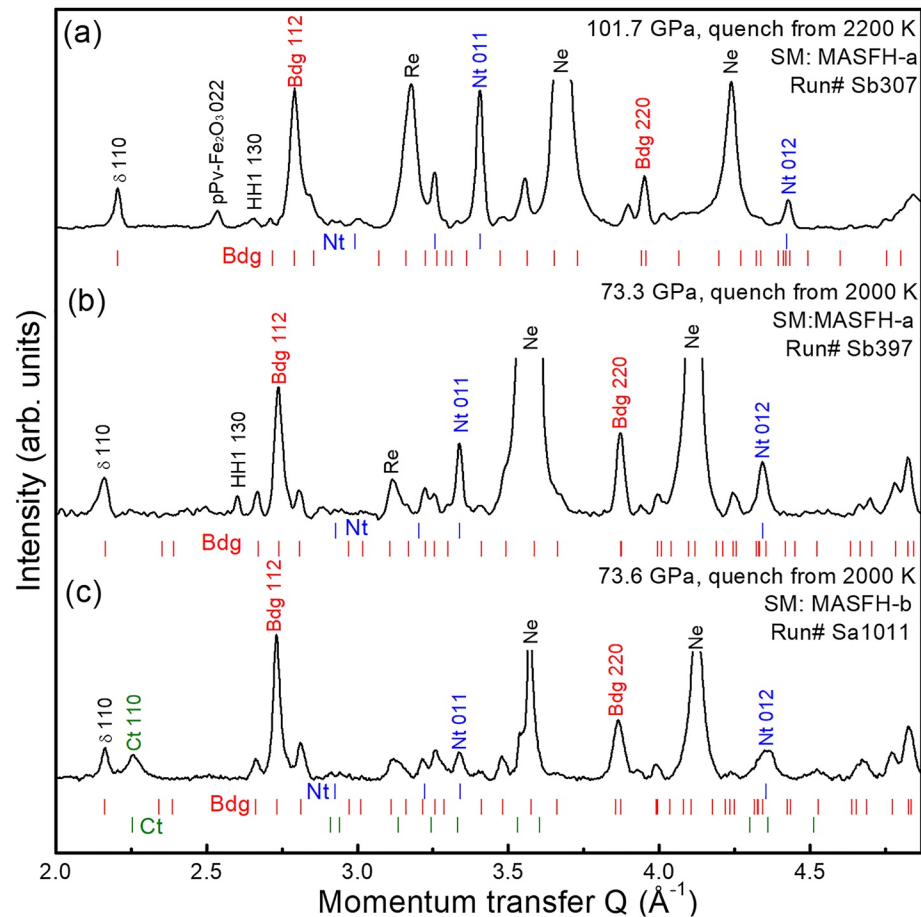


Figure 1. Representative X-ray diffraction patterns of the run products in the MAFSH system at high P and room T after laser heating. The phase assemblages are identified as (a) coexisting Nt-phase, Bdg, δ -phase, HH1-phase, and pPv- Fe_2O_3 , (b) coexisting Nt-phase, Bdg, δ -phase and HH1-phase, and (c) coexisting Nt-phase, Ct-phase, Bdg, and δ -phase. Phase labels are the same as in Table 1. The unit-cell parameters of the Nt-phase and Bdg are shown in Table S1 in Supporting Information S1.

intensity. However, the conventional high-pressure silica phase including stishovite, CaCl_2 -type phase (Ct-phase) and seifertite were not observed as a dominant silica mineral in the phase assemblages. It is worth noting that the Nt-phase with its characteristic reflections 011 and 012 can be well recognized (Figure 1). Importantly, the multigrain XRD analysis allowed us to unambiguously identify such a Nt-phase in the multiphase assemblages (Figure S3 in Supporting Information S1). For instance, up to 24 reflections were indexed for the individual grains of the Nt-phase at 101.7 GPa (Run# Sb307, Table S2 in Supporting Information S1). In general, the phase assemblages can be identified as the coexisting Nt-phase, Bdg, δ -phase and iron-rich phase(s). An exception was found with the additional Ct-phase, which could likely be attributed to a relatively higher temperature of 2200 K at 97 GPa (Run# Sb355, Figure S2 in Supporting Information S1), possibly resulting in a partial conversion from the Nt-phase to the Ct-phase. In this run, we observed the post-perovskite-type Fe_2O_3 phase (pPv- Fe_2O_3) rather than a hexagonal iron-rich phase, referred to as HH1-phase (L. Liu et al., 2022), which was present in the other runs. (Note that a $(\text{Mg}, \text{Fe})_2\text{O}_{3+\delta}$ ($0 < \delta < 1$) phase with similar unit-cell parameters was named as “OE-phase” by J. Liu et al. (2020); the iron oxide endmember was named as “ η -phase” in Chen et al. (2020) and as $\text{Fe}_{6.32}\text{O}_9$ in Koemets et al. (2021).) The Nt-phase cannot be preserved after decompression to ambient conditions, which is consistent with the unquenchable nature of the water-bearing Al-free Nt-phase in the previous study of Nisir et al. (2020).

To our knowledge, the Nt-phase was found for the first time in a hydrated multicomponent basaltic composition. Previous studies on dry basaltic compositions reported the formation of the Ct-phase under comparable high P - T conditions (Hirose et al., 2005; Ricolleau et al., 2010). To further understand the role of water in the formation

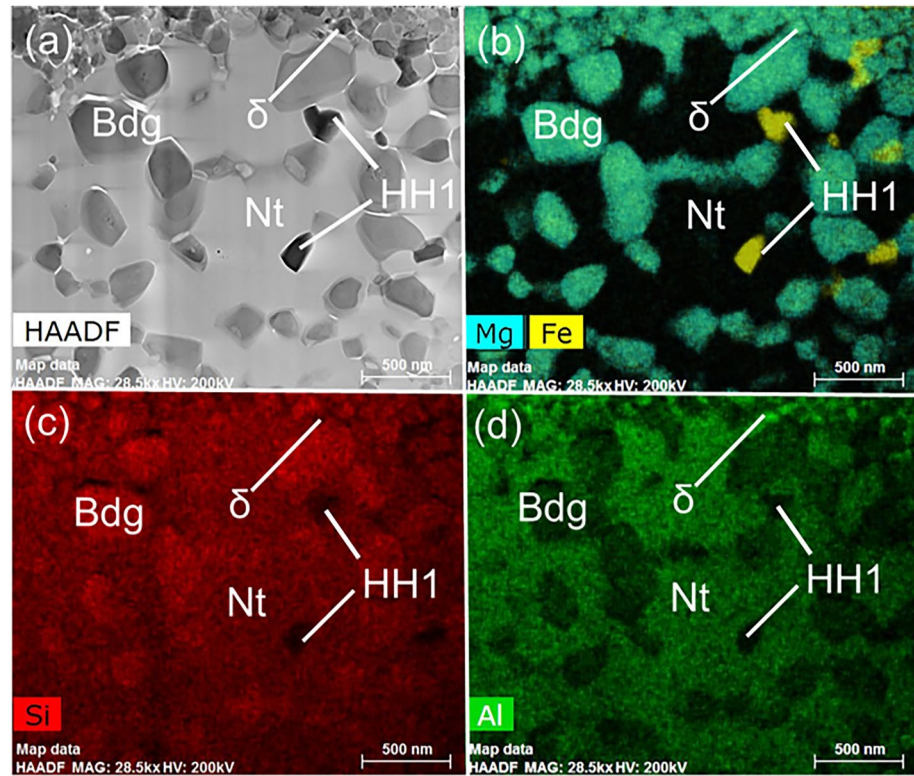


Figure 2. Transmission electron microscopy-energy dispersive X-ray spectroscopy images of the run products recovered from 84 GPa to 2,000 K. (a) High-angle annular dark field image. Compositional mapping images of (b) Fe + Mg, (c) Si, and (d) Al. Elements Si, Mg, Al, and Fe are shown in red, cyan, green, and yellow, respectively.

of the Nt-phase, we conducted a comparison experiment on the relatively drier sample with reduced bulk water content (MAFSH-b, containing ~ 1 wt% water) at 84 GPa and 2,000 K. As shown in Figure 1c, the run products can be identified as the coexistence of the Nt-phase, Ct-phase, Bdg, and δ -phase (Run# Sa1011). Under nearly the same P - T conditions (Run# Sb397, Figure 1b), the Ct-phase was undetectable in the wetter sample (MAFSH-a, containing ~ 4 wt% H_2O). These combined results indicate that the amount and stability of silica phases (e.g., Nt-phase and Ct-phase) depend on the water content of the starting material. Walter et al. (2015) studied the phase relation of the model hydrated mafic and basaltic rocks in the MgO - SiO_2 - H_2O and MgO - Al_2O_3 - SiO_2 - H_2O systems using XRD measurements on the recovered assemblages. We note that the stishovite 110 reflection in their basaltic sample considerably decreases in intensity from 49 to 60 GPa and above, and this characteristic reflection is even absent at 94 GPa. One possible explanation is the formation of Nt-phase at high pressure, which is unquenchable at ambient conditions.

Chemical analysis using TEM-EDS was performed on two representative samples recovered from 84 GPa to 2,000 K (Run# Sb397) and from 113 GPa to 2,200 K (Run# Sb307), respectively. As shown in Figure 2, the coexisting Nt-phase, Bdg, δ -phase, and Fe-rich HH1-phase can be clarified on the basis of their chemical compositions, in agreement with the XRD results. The Nt-phase and Bdg are major phases in the quenched products. As summarized in Table S3 in Supporting Information S1, a significant amount of Al_2O_3 (~ 32.4 and 24.4 wt%) together with a modest amount of Fe_2O_3 (~ 3.7 and 4.0 wt%) and/or MgO (~ 1.3 wt%) were clearly demonstrated in the recovered silica-rich phase from 84 GPa, 2,000 K and 113 GPa, 2,200 K, respectively, which is derived from the high-pressure Nt-phase. Meanwhile, the coexisting Bdg is Al-depleted with the Al_2O_3 contents of ~ 7.6 and ~ 6.4 wt% for the samples recovered from 84 to 113 GPa, respectively: these alumina contents in Bdg are significantly smaller than 14–15 wt% in dry MORB (Hirose & Fei, 2002; Litasov & Ohtani, 2005; Ricolleau et al., 2010). The Al component is preferentially incorporated into the Al-rich Nt-phase rather than the Al-depleted Bdg phase. The partition coefficient $D_{Nt/Bdg}$ of Al_2O_3 is calculated as ~ 5 .

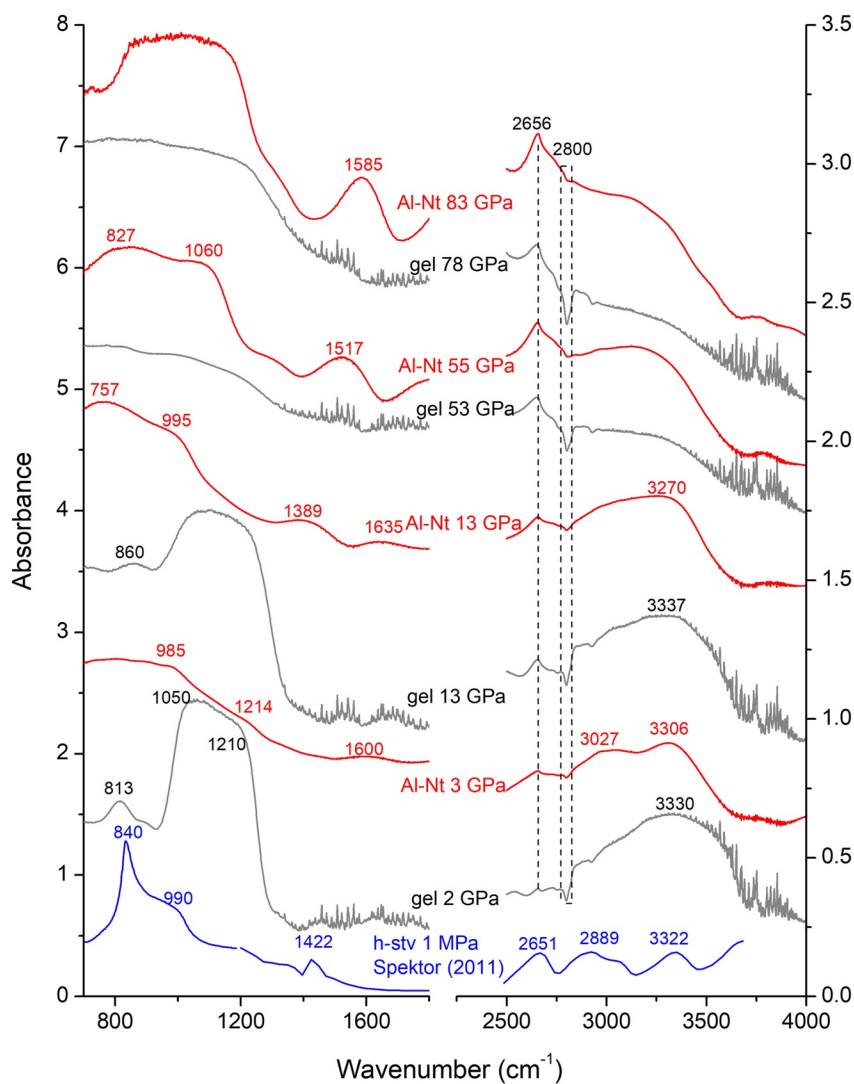


Figure 3. Infrared (IR) spectra of starting ASH gel sample during compression (gray), synthetic Al-rich Nt-phase during decompression (red) and hydrous stishovite (blue) from Spektor et al. (2011). The change of scale in the absorbance axis is utilized to illustrate the fundamental OH stretching vibration region. The use of an empty diamond anvil cell at ambient conditions as the reference spectrum gives rise to an increased background in the high-frequency region at $P > 50$ GPa. The peak at $2,656\text{ cm}^{-1}$ (guided by dashed line) and the trough at $2,800\text{ cm}^{-1}$ (guided by dashed frame) are artifacts (note that their positions were unchanged with pressure), which are caused by the changes in absorption from the diamond anvil interferes and by CH stretching vibration from the baseline correction, respectively. In the IR spectra of the gel sample, the sharp absorption peaks around $1,600$ and $3,700\text{ cm}^{-1}$ are attributed to atmospheric water due to the non-perfect purging of the Bruker Hyperion 2000 microscope. IR spectra are vertically shifted for better comparison.

High-pressure IR spectroscopic investigations were performed on both the starting ASH gel sample and a synthetic pure Al-rich Nt-phase (Al:Si = 3:7) for comparison. As seen in Figure 3, IR spectra featured strong bands in the range of $700\text{--}900$ and $950\text{--}1,300\text{ cm}^{-1}$, which are associated with the Si–O symmetric and asymmetric stretching vibrations, respectively (Kamitsos et al., 1993). At low pressures, bands corresponding to the Si–O symmetric stretching vibration in the Al-rich Nt-phase (e.g., 785 cm^{-1} at 13 GPa) were in the lower-frequency region relative to the previously reported hydrous stishovite (e.g., 840 cm^{-1} at 1 MPa; Spektor et al., 2011), reflecting increased Si–O distances in SiO_6 octahedra. For the Al-rich Nt-phase, a distinct band centered at $1,585\text{ cm}^{-1}$ at ~ 80 GPa largely red shifted to approximately $1,214\text{ cm}^{-1}$ as a shoulder at 3 GPa, whose origin is unknown. In addition, a weak band at $1,600\text{ cm}^{-1}$ at 3 GPa blue shifted to $1,635\text{ cm}^{-1}$ at 13 GPa, which can be assigned to OH bending vibration belonging to Al-rich Nt-phase instead of molecular water, because the frequency of this mode in molecular water is insensitive to pressure, remaining at $\sim 1,600\text{ cm}^{-1}$ up to 40 GPa (Song et al., 1999).

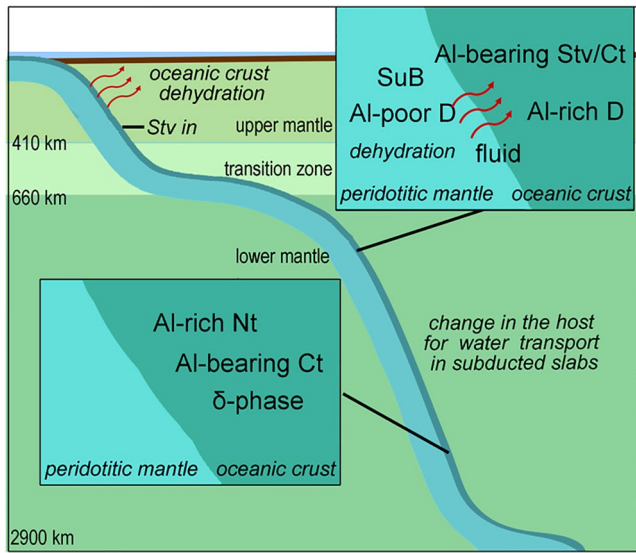


Figure 4. Potential mechanism for water transport into the lower mantle via subduction of lithospheric plates. Nearly complete dehydration of oceanic crust is expected to occur at depths <250 km. Water may be essentially stored in post-serpentine dense hydrous phases in peridotitic portion of the coldest subducting slabs, passing through the transition zone. At the top of lower mantle, dehydration of Al-poor phase D and superhydrous phase B (SuB) in peridotitic mantle occurs, and the released water possibly migrates to the basaltic oceanic crust layer, forming water-bearing phases such as Al-bearing stishovite, Ct-phase, and hydrous Al-rich phase D at the shallow lower mantle. At the middle lower mantle, the water-bearing phases can be changed into Al-rich Nt-phase, δ -phase, and/or aluminous Ct-phase in the basaltic portion of slabs.

These results indicate the complete reaction to produce the Al-rich Nt-phase without detectable water inclusion in grain boundaries after CO₂ laser heating, and released water if it existed, might be diluted into the Ar medium near the cold chamber edge. The broad bands in the range of 2,700–3,700 cm⁻¹ are ascribed to OH stretching vibrations. The OH bands became weak in intensity in the starting gel sample at $P > 50$ GPa, while the OH bands in the Al-rich Nt-phase could be clearly observed, although there was a great background due to the use of empty DAC at ambient conditions as reference spectrum (Figure 3). Notably, there were at least two OH stretching modes with the maximums of 3,027 and 3,306 cm⁻¹ in the Al-rich Nt-phase at 3 GPa, possibly representing two types of hydrogen sites in Al-rich Nt-phase with different frequency and absorbance responses to pressure. Compared with ice VII (Song et al., 1999), Al-bearing stishovite (Litasov et al., 2007) and hydrous stishovite (Spektor et al., 2011), Al-rich Nt-phase showed distinctive high-pressure IR features, especially in OH bending and stretching vibrations regions, providing direct evidence for the existence of structural water in Al-rich Nt-phase (Figure S7 in Supporting Information S1).

As Al-rich Nt-phase is unquenchable to ambient conditions, we estimated the water content by the method of Paterson (1982) based on the spectrum at 3 GPa (Text S2 in Supporting Information S1). When applying Paterson's method to a high-pressure sample, a major uncertainty comes from the thickness of the sample. Assuming the compressed sample thickness of ~5 to 10 μ m, the water content is calculated to be ~1.5 to 3 wt%. The contribution of the background from our correction using the spectrum of the empty DAC at ambient pressure can give rise to an overestimation of up to 10% of the water content (Figure S6 in Supporting Information S1). As application of Paterson's method from ambient to high pressure has not been well evaluated, the estimated water content should be viewed as preliminary.

4. Geophysical Implications

Hydration of rocks can have a profound effect on the phase assemblages and mineral chemistry. Previous studies showed that the Al₂O₃ content in aluminous stishovite is generally higher in hydrous than dry oceanic crust under the shallow lower mantle conditions (Litasov & Ohtani, 2005). Our results show that Al-rich Nt-phase can hold ~24.4 to 32.4 wt% Al₂O₃ and ~1.5 to 3 wt% H₂O in the middle or deep lower mantle; the coexisting Bdg contains ~6.4 to 7.6 wt% Al₂O₃, which is much lower than the Al₂O₃ content in Bdg in a dry MORB (14–15 wt%: Hirose & Fei, 2002; Litasov & Ohtani, 2005; Ricolleau et al., 2010). Ishii et al. (2022) showed that both alumina and hydrogen preferentially partition into hydrous phases (phases D and δ -H) rather than the coexisting Bdg in the MgSiO₃-Al₂O₃-H₂O system. In water saturated conditions, Chen et al. (2020) found that water reacts with Al-bearing CaSiO₃ to produce coexisting hydrous δ -AlO₂H and a potential water-bearing Al-depleted CaSiO₃ phase.

Oceanic crust in subducted slabs is expected to be nearly dehydrated at depths of less than 250 km (Okamoto & Maruyama, 2004), shallower than the depths where stishovite first crystallizes at ~300 km. Water may be essentially stored in post-serpentine dense hydrous phases in the peridotitic portion of the coldest subducting slabs, passing through the transition zone. The global water flux beyond ~250 km and into the deeper mantle is predicted to be near one ocean mass over the age of the Earth, while only 1/3 of that is estimated to be stored in the peridotitic portion of the slabs (Van Keken et al., 2011). Based on previous and current studies, we suggest a potential mechanism for the water transport into the deep Earth's interior via subduction of hydrated lithospheric plates (Figure 4).

The water storage capacities of the most modally dominant nominally anhydrous minerals were not fully constrained but thought to be nearly dry under lower mantle conditions except for silica, although a potential water-bearing CaSiO₃ was suggested (Chen et al., 2020), which is not included in our model basaltic compositions

for simplicity. At the top of the lower mantle, dehydration of superhydrous phase B (Ohtani et al., 2001) and Al-poor phase D (Nishi et al., 2014) is expected to occur in most subducting peridotitic rocks due to their low temperature stability. If the movement of the released aqueous fluids is efficient, water can potentially migrate into the adjacent basaltic layer of the descending slabs, forming hydrated (possibly aluminous) silica and/or Al-rich phase D in the basaltic assemblages (Walter, 2021). Recent experimental studies showed that Al-free stishovite might contain weight percent levels of water along a mantle geotherm (Lin et al., 2020; Nisr et al., 2020). In addition, Al-rich phase D will transform to δ -phase or undergo dehydration melting with increasing depth (Xu & Inoue, 2019). If hydrated slabs survive and reach to the middle lower mantle, water-bearing phase(s) would likely change into Al-rich Nt-phase, δ -phase and/or aluminous Ct-phase in the basaltic portion of these slabs, which is dependent on water availability, temperature, extent of the interplay with surrounding minerals. Importantly, with the high modal abundance in basaltic slabs (e.g., ~20 wt% in MORB, Hirose et al., 2005), Al-rich Nt-phase has comparable water storage capability to ultrahydrous stishovite, accommodating weight percent levels of water in the middle and deep lower mantle. Furthermore, hydrated iron-rich oxide including HH phase (L. Zhang et al., 2018) and pyrite- FeO_2H_x (Hu et al., 2016; J. Liu et al., 2017; Nishi et al., 2017) could retain water even well beyond the average mantle geotherm. The progressive hydration of recycled oceanic crust due to crystallization of water-bearing (Al-rich) silica, Al-rich silicate and iron-rich oxides in the lower mantle will likely provide a continuous link to convey water to the base of the lower mantle. The steep temperature increase at the core mantle boundary could trigger melting, forming FeO and FeH components (Mao et al., 2017; Nishi et al., 2020; Piet et al., 2020). The water supply via subduction of slabs could possibly be the vital source for hydrogenation of Earth's core.

Data Availability Statement

The experimental data used in this manuscript can be found in a FAIR-compliant data repository at <https://doi.org/10.5281/zenodo.6474489>.

Acknowledgments

This work was supported from the National Natural Science Foundation of China (NSFC) (Grant Nos 41902033 and 42150103). The authors acknowledge Deutsches Elektronen Synchrotron (DESY, Hamburg, Germany), a member of the Helmholtz Association HGF, and Shanghai Synchrotron Radiation Facility (SSRF) for the provision of experimental facilities. Portions of this research were carried out at the light source PETRA III at DESY. Portions of this work were performed at BL15U1 and BL06B1 at SSRF. The authors appreciate comments from the two anonymous reviewers.

References

- Akahama, Y., & Kawamura, H. (2004). High-pressure Raman spectroscopy of diamond anvils to 250 GPa: Method for pressure determination in the multimegabar pressure range. *Journal of Applied Physics*, 96(7), 3748–3751. <https://doi.org/10.1063/1.1778482>
- Bolfan-Casanova, N., Keppler, H., & Rubie, D. C. (2000). Water partitioning between nominally anhydrous minerals in the MgO-SiO₂-H₂O system up to 24 GPa: Implications for the distribution of water in the Earth's mantle. *Earth and Planetary Science Letters*, 182(3–4), 209–221. [https://doi.org/10.1016/S0012-821X\(00\)00244-2](https://doi.org/10.1016/S0012-821X(00)00244-2)
- Bromiley, G. D., Bromiley, F. A., & Bromiley, D. W. (2006). On the mechanisms for H and Al incorporation in stishovite. *Physics and Chemistry of Minerals*, 33(8–9), 613–621. <https://doi.org/10.1007/s00269-006-0107-9>
- Chen, H., Leinenweber, K., Prakapenka, V., Prescher, C., Meng, Y., Bechtel, H., et al. (2020). Possible H₂O storage in the crystal structure of CaSiO₃ perovskite. *Physics of the Earth and Planetary Interiors*, 299(August 2019), 106412. <https://doi.org/10.1016/j.pepi.2019.106412>
- Fei, Y., Ricolleau, A., Frank, M., Mibe, K., Shen, G., & Prakapenka, V. (2007). Toward an internally consistent pressure scale. *Proceedings of the National Academy of Sciences*, 104(22), 9182–9186. <https://doi.org/10.1073/pnas.0609013104>
- Finger, L. W., Hazen, R. M., Zou, G., Mao, H. K., & Bell, P. M. (1981). Structure and compression of crystalline argon and neon at high pressure and room temperature. *Applied Physics Letters*, 39(11), 892–894. <https://doi.org/10.1063/1.92597>
- Grand, S. P. (2002). Mantle shear-wave tomography and the fate of subducted slabs. *Philosophical Transactions of the Royal Society A: Mathematical, Physical & Engineering Sciences*, 360(1800), 2475–2491. <https://doi.org/10.1098/rsta.2002.1077>
- Hirose, K., & Fei, Y. (2002). Subsolidus and melting phase relations of basaltic composition in the uppermost lower mantle. *Geochimica et Cosmochimica Acta*, 66(12), 2099–2108. [https://doi.org/10.1016/S0016-7037\(02\)00847-5](https://doi.org/10.1016/S0016-7037(02)00847-5)
- Hirose, K., Takafuji, N., Sata, N., & Ohishi, Y. (2005). Phase transition and density of subducted MORB crust in the lower mantle. *Earth and Planetary Science Letters*, 237(1–2), 239–251. <https://doi.org/10.1016/j.epsl.2005.06.035>
- Hu, Q., Kim, D. Y., Yang, W., Yang, L., Meng, Y., Zhang, L., & Mao, H. K. (2016). FeO₂ and FeOOH under deep lower-mantle conditions and Earth's oxygen-hydrogen cycles. *Nature*, 534(7606), 241–244. <https://doi.org/10.1038/nature18018>
- Ishii, T., Ohtani, E., & Shatskiy, A. (2022). Aluminum and hydrogen partitioning between bridgmanite and high-pressure hydrous phases: Implications for water storage in the lower mantle. *Earth and Planetary Science Letters*, 583, 117441. <https://doi.org/10.1016/j.epsl.2022.117441>
- Iwamori, H. (2004). Phase relations of peridotites under H₂O-saturated conditions and ability of subducting plates for transportation of H₂O. *Earth and Planetary Science Letters*, 227(1–2), 57–71. <https://doi.org/10.1016/j.epsl.2004.08.013>
- Kamitsos, E. I., Patsis, A. P., & Kordas, G. (1993). Infrared-reflectance spectra of heat-treated sol-gel-derived silica. *Physical Review B*, 48(17), 12499–12505. <https://doi.org/10.1103/PhysRevB.48.12499>
- Kawazoe, T., Ohira, I., Ishii, T., Ballaran, T. B., McCammon, C., Suzuki, A., & Ohtani, E. (2017). Single crystal synthesis of δ -(Al, Fe)OOH. *American Mineralogist*, 102(9), 1953–1956. <https://doi.org/10.2138/am-2017-6153>
- Koemets, E., Fedotenko, T., Khandarkhaeva, S., Bykov, M., Bykova, E., Thielmann, M., et al. (2021). Chemical stability of FeOOH at high pressure and temperature, and oxygen recycling in early Earth history. *European Journal of Inorganic Chemistry*, 2021(30), 3048–3053. <https://doi.org/10.1002/ejic.202100274>
- Koňopková, Z., Morgenroth, W., Husband, R., Giordano, N., Pakhomova, A., Gutowski, O., et al. (2021). Laser heating system at the Extreme conditions beamline, P02.2, PETRA III. *Journal of Synchrotron Radiation*, 28(6), 1747–1757. <https://doi.org/10.1107/S1600577521009231>

- Lin, Y., Hu, Q., Meng, Y., Walter, M., & Mao, H. K. (2020). Evidence for the stability of ultrahydrous stishovite in Earth's lower mantle. *Proceedings of the National Academy of Sciences of the United States of America*, 117(1), 184–189. <https://doi.org/10.1073/pnas.1914295117>
- Litasov, K. D., Kagi, H., Shatskiy, A., Ohtani, E., Lakshatnov, D. L., Bass, J. D., & Ito, E. (2007). High hydrogen solubility in Al-rich stishovite and water transport in the lower mantle. *Earth and Planetary Science Letters*, 262(3–4), 620–634. <https://doi.org/10.1016/j.epsl.2007.08.015>
- Litasov, K. D., & Ohtani, E. (2005). Phase relations in hydrous MORB at 18–28 GPa: Implications for heterogeneity of the lower mantle. *Physics of the Earth and Planetary Interiors*, 150(4), 239–263. <https://doi.org/10.1016/j.pepi.2004.10.010>
- Liu, J., Hu, Q., Young Kim, D., Wu, Z., Wang, W., Xiao, Y., et al. (2017). Hydrogen-bearing iron peroxide and the origin of ultralow-velocity zones. *Nature*, 551(7681), 494–497. <https://doi.org/10.1038/nature24461>
- Liu, J., Wang, C., Lv, C., Su, X., Liu, Y., Tang, R., et al. (2020). Evidence for oxygenation of Fe-Mg oxides at mid-mantle conditions and the rise of deep oxygen. *National Science Review*, 8(4), nwaa096. <https://doi.org/10.1093/nsr/nwaa096>
- Liu, L., Yang, Z., Yuan, H., Meng, Y., Giordano, N., Sun, J., et al. (2022). Stability of a mixed-valence hydrous iron-rich oxide: Implications for water storage and dynamics in the deep lower mantle. *Journal of Geophysical Research: Solid Earth*, 127(5), e2022JB024288. <https://doi.org/10.1029/2022JB024288>
- Mao, H. K., Hu, Q., Yang, L., Liu, J., Kim, D. Y., Meng, Y., et al. (2017). When water meets iron at Earth's core-mantle boundary. *National Science Review*, 4(6), 870–878. <https://doi.org/10.1093/nsr/nwx109>
- Nishi, M., Irifune, T., Tsuchiya, J., Tange, Y., Nishihara, Y., Fujino, K., & Higo, Y. (2014). Stability of hydrous silicate at high pressures and water transport to the deep lower mantle. *Nature Geoscience*, 7(3), 224–227. <https://doi.org/10.1038/ngeo2074>
- Nishi, M., Kuwayama, Y., Hatakeyama, T., Kawaguchi, S., Hirao, N., Ohishi, Y., & Irifune, T. (2020). Chemical reaction between metallic iron and a limited water supply under pressure: Implications for water behavior at the core-mantle boundary. *Geophysical Research Letters*, 47(19), 1–7. <https://doi.org/10.1029/2020GL089616>
- Nishi, M., Kuwayama, Y., Tsuchiya, J., & Tsuchiya, T. (2017). The pyrite-type high-pressure form of FeOOH. *Nature*, 547(7662), 205–208. <https://doi.org/10.1038/nature22823>
- Nishi, M., Tsuchiya, J., Kuwayama, Y., Arimoto, T., Tange, Y., Higo, Y., et al. (2019). Solid solution and compression behavior of hydroxides in the lower mantle. *Journal of Geophysical Research: Solid Earth*, 124(10), 10231–10239. <https://doi.org/10.1029/2019JB018146>
- Nisr, C., Chen, H., Leinenweber, K., Chizmeshya, A., Prakapenka, V. B., Prescher, C., et al. (2020). Large H₂O solubility in dense silica and its implications for the interiors of water-rich planets. *Proceedings of the National Academy of Sciences*, 117(18), 9747–9754. <https://doi.org/10.1073/pnas.1917448117>
- Ohira, I., Ohtani, E., Sakai, T., Miyahara, M., Hirao, N., Ohishi, Y., & Nishijima, M. (2014). Stability of a hydrous δ -phase, AlOOH-MgSiO₂(OH)₂, and a mechanism for water transport into the base of lower mantle. *Earth and Planetary Science Letters*, 401, 12–17. <https://doi.org/10.1016/j.epsl.2014.05.059>
- Ohtani, E. (2020). The role of water in Earth's mantle. *National Science Review*, 7(1), 224–232. <https://doi.org/10.1093/nsr/nwz071>
- Ohtani, E. (2021). Hydration and dehydration in Earth's interior. *Annual Review of Earth and Planetary Sciences*, 49(1), 253–278. <https://doi.org/10.1146/annurev-earth-080320-062509>
- Ohtani, E., Toma, M., Litasov, K., Kubo, T., & Suzuki, A. (2001). Stability of dense hydrous magnesium silicate phases and water storage capacity in the transition zone and lower mantle. *Physics of the Earth and Planetary Interiors*, 124(1–2), 105–117. [https://doi.org/10.1016/S0031-9201\(01\)00192-3](https://doi.org/10.1016/S0031-9201(01)00192-3)
- Ohtani, E., Yuan, L., Ohira, I., Shatskiy, A., & Litasov, K. (2018). Fate of water transported into the deep mantle by slab subduction. *Journal of Asian Earth Sciences*, 167, 2–10. <https://doi.org/10.1016/j.jseaes.2018.04.024>
- Okamoto, K., & Maruyama, S. (2004). The eclogite-garnetite transformation in the MORB + H₂O system. *Physics of the Earth and Planetary Interiors*, 146(1–2), 283–296. <https://doi.org/10.1016/j.pepi.2003.07.029>
- Paterson, M. S. (1982). The determination of hydroxyl by infrared adsorption in quartz, silicate glasses and similar materials. *Bulletin de Mineralogie*, 105(1), 20–29. <https://doi.org/10.3406/bulmi.1982.7582>
- Pawley, A. R., McMillan, P. F., & Holloway, J. R. (1993). Hydrogen in stishovite, with implications for mantle water content. *Science*, 261(5124), 1024–1026. <https://doi.org/10.1126/science.261.5124.1024>
- Pearson, D. G., Brenker, F. E., Nestola, F., McNeill, J., Nasdala, L., Hutchison, M. T., et al. (2014). Hydrous mantle transition zone indicated by ringwoodite included within diamond. *Nature*, 507(7491), 221–224. <https://doi.org/10.1038/nature13080>
- Perrillat, J.-P., Ricolleau, A., Daniel, I., Fiquet, G., Mezouar, M., Guignot, N., & Cardon, H. (2006). Phase transformations of subducted basaltic crust in the upmost lower mantle. *Physics of the Earth and Planetary Interiors*, 157(1–2), 139–149. <https://doi.org/10.1016/j.pepi.2006.04.001>
- Piet, H., Leinenweber, K. D., Tappan, J., Greenberg, E., Prakapenka, V. B., Buseck, P. R., & Sang-Heon, S. (2020). Dehydration of δ -AlOOH in Earth's deep lower mantle. *Minerals*, 10(4), 384. <https://doi.org/10.3390/min10040384>
- Ricolleau, A., Perrillat, J. P., Fiquet, G., Daniel, I., Matas, J., Addad, A., et al. (2010). Phase relations and equation of state of a natural MORB: Implications for the density profile of subducted oceanic crust in the Earth's lower mantle. *Journal of Geophysical Research*, 115(8), B08202. <https://doi.org/10.1029/2009JB006709>
- Song, M., Yamawaki, H., Fujihisa, H., Sakashita, M., & Aoki, K. (1999). Infrared absorption study of Fermi resonance and hydrogen-bond symmetrization of ice up to 141 GPa. *Physical Review B: Condensed Matter and Materials Physics*, 60(18), 12644–12650. <https://doi.org/10.1103/PhysRevB.60.12644>
- Spekter, K., Nysten, J., Stoyanov, E., Navrotsky, A., Hervig, R. L., Leinenweber, K., et al. (2011). Ultrahydrous stishovite from high-pressure hydrothermal treatment of SiO₂. *Proceedings of the National Academy of Sciences of the United States of America*, 108(52), 20918–20922. <https://doi.org/10.1073/pnas.1117152108>
- Tschauner, O., Huang, S., Greenberg, E., Prakapenka, V. B., Ma, C., Rossman, G. R., et al. (2018). Ice-VII inclusions in diamonds: Evidence for aqueous fluid in Earth's deep mantle. *Science*, 359(6380), 1136–1139. <https://doi.org/10.1126/science.aao3030>
- Van Keken, P. E., Hacker, B. R., Syracuse, E. M., & Abers, G. A. (2011). Subduction factory: 4. Depth-dependent flux of H₂O from subducting slabs worldwide. *Journal of Geophysical Research*, 116(1), B01401. <https://doi.org/10.1029/2010JB007922>
- Walter, M. J. (2021). Water transport to the core-mantle boundary. *National Science Review*, 8(4), 8–11. <https://doi.org/10.1093/nsr/nwab007>
- Walter, M. J., Thomson, A. R., Wang, W., Lord, O. T., Ross, J., McMahon, S. C., et al. (2015). The stability of hydrous silicates in Earth's lower mantle: Experimental constraints from the systems MgO-SiO₂-H₂O and MgO-Al₂O₃-SiO₂-H₂O. *Chemical Geology*, 418, 16–29. <https://doi.org/10.1016/j.chemgeo.2015.05.001>
- Wirth, R., Vollmer, C., Brenker, F., Matsyuk, S., & Kaminsky, F. (2007). Inclusions of nanocrystalline hydrous aluminium silicate 'Phase Egg' in superdeep diamonds from Juina (Mato Grosso State, Brazil). *Earth and Planetary Science Letters*, 259(3–4), 384–399. <https://doi.org/10.1016/j.epsl.2007.04.041>
- Xu, C., & Inoue, T. (2019). Melting of Al-rich phase D up to the uppermost lower mantle and transportation of H₂O to the deep Earth. *Geochemistry, Geophysics, Geosystems*, 20(9), 4382–4389. <https://doi.org/10.1029/2019GC008476>

- Yuan, H., Zhang, L., Ohtani, E., Meng, Y., Greenberg, E., & Prakapenka, V. B. (2019). Stability of Fe-bearing hydrous phases and element partitioning in the system $\text{MgO-Al}_2\text{O}_3\text{-Fe}_2\text{O}_3\text{-SiO}_2\text{-H}_2\text{O}$ in Earth's lowermost mantle. *Earth and Planetary Science Letters*, 524, 115714. <https://doi.org/10.1016/j.epsl.2019.115714>
- Zhang, L., Yuan, H., Meng, Y., & Mao, H. K. (2018). Discovery of a hexagonal ultradense hydrous phase in (Fe, Al)OOH. *Proceedings of the National Academy of Sciences of the United States of America*, 115(12), 2908–2911. <https://doi.org/10.1073/pnas.1720510115>
- Zhang, L., Yuan, H., Meng, Y., & Mao, H. K. (2019). Development of high-pressure multigrain X-ray diffraction for exploring the Earth's interior. *Engineering*, 5(3), 441–447. <https://doi.org/10.1016/j.eng.2019.02.004>
- Zhang, L. L., Yan, S., Jiang, S., Yang, K., Wang, H., He, S. M., et al. (2015). Hard X-ray micro-focusing beamline at SSRF. *Nuclear Science and Techniques*, 26(6), 1–8. <https://doi.org/10.13538/j.1001-8042/nst.26.060101>
- Zhao, D. (2012). Tomography and dynamics of Western-Pacific subduction zones. *Monographs on Environment, Earth and Planets*, 1(1), 1–70. <https://doi.org/10.5047/meep.2012.00101.0001>

References From the Supporting Information

- Hamilton, D. L., & Henderson, C. M. B. (1968). The preparation of silicate compositions by a gelling method. *Mineralogical Magazine and Journal of the Mineralogical Society*, 36(282), 832–838. <https://doi.org/10.1180/minmag.1968.036.282.11>
- Schmidt, S. (2014). GrainSpotter: A fast and robust polycrystalline indexing algorithm. *Journal of Applied Crystallography*, 47(1), 276–284. <https://doi.org/10.1107/S1600576713030185>
- Sørensen, H. O., Schmidt, S., Wright, J. P., Vaughan, G. B. M., Techert, S., Garman, E. F., et al. (2012). Multigrain crystallography. *Zeitschrift für Kristallographie*, 227(1), 63–78. <https://doi.org/10.1524/zkri.2012.1438>